

1 **The origin of the Zhangjialong tungsten deposit, South China: Implications for W-Sn mineralization**
2 **in large granite batholiths.**

3 Shunda Yuan¹, A.E. Williams-Jones², Jingwen Mao¹, Panlao Zhao¹, Chen Yan¹, Dongliang Zhang³

4 1. *MLR Key Laboratory of Metallogeny and Mineral Assessment, Institute of Mineral Resources, Chinese*
5 *Academy of Geological Sciences, Beijing 100037, China*

6 2. *Department of Earth and Planetary Sciences, McGill University, 3450 University Street, Montreal H3A*
7 *0E8, Canada*

8 3. *Key Laboratory of Continental Dynamics, Department of Geology, School of Geosciences and*
9 *Info-physics, Central South University, Changsha, 410083, PR China*

10 **Abstract.** The Nanling region is the largest W-Sn metallogenic district in the World and hosts a number
11 of giant W-Sn deposits, all of which are spatially and genetically associated with highly evolved Mesozoic
12 granitic stocks. Volumetrically, however, Caledonian granites (Paleozoic), mainly batholiths, approach their
13 Mesozoic equivalents in importance and have been the target of recent exploration. This has resulted in the
14 discovery of a number of economic tungsten deposits in or near these granite batholiths, including the giant
15 Zhangjialong deposit, which is located on the southern margin of the Caledonian Penggongmiao granite
16 batholith. The unresolved question is whether or not this is evidence for an important Caledonian epoch of
17 W-Sn mineralization. In this contribution, we report the results of high precision SIMS zircon U-Pb,
18 muscovite Ar-Ar, and molybdenite Re-Os age determinations that constrain the timing relationships among
19 granitic magmatism, greisenization and tungsten mineralization related to the Zhangjialong deposit. The
20 molybdenite Re-Os age of the tungsten mineralization is 160.2 ± 2.2 Ma, which is similar to, albeit slightly
21 older than, the muscovite Ar-Ar age of the greisen (153.5 ± 1.0 Ma). These ages, however, are considerably
22 younger than the zircon SIMS U-Pb age of 441.3 ± 2.4 Ma for the spatially associated granite. These data

23 demonstrate that the tungsten mineralization and greisenization of the Zhangjialong W deposit is of Late
24 Jurassic rather than Silurian age, which precludes a temporal and genetic link between the hydrothermal
25 tungsten mineralization and the regional Caledonian magmatism. Instead, the tungsten mineralization is
26 interpreted to be related to a hidden Late Jurassic granitic pluton. A compilation of published whole-rock
27 geochemical data indicate that the large granite batholiths are less differentiated than the W-Sn bearing granite
28 stocks, irrespective of whether they are Paleozoic or Mesozoic in age. This suggests that the metallogenic
29 potential of the large granitic batholiths is limited, and that W-Sn deposits hosted within granite batholiths
30 are likely to be genetically related to highly evolved granitic stocks that in some cases have not been exposed.
31 **Keywords** Re-Os Molybdenite; Ar-Ar muscovite; SIMS zircon U-Pb; Caledonian batholiths; Late Mesozoic
32 tungsten mineralization; Nanling region

33 **1. Introduction**

34 Most giant W-Sn deposits are temporally, spatially and genetically related to highly evolved granitic
35 stocks (Sillitoe et al., 1975; Romer and Kroner, 2016; Korges et al., 2017). However, there are also many W-
36 Sn deposits within or at the margins of large granitic batholiths (Willis-Richards and Jackson, 1989; Sun and
37 Higgins, 1996; Yokart et al., 2003; Hulsbosch et al., 2016), for which a genetic relationship with the spatially
38 associated granite is unclear (Kelly and Turneure, 1970; Kelly and Rye, 1979; Hulsbosch et al., 2016). This
39 is an important issue to resolve, because granitic batholiths provide very large exploration targets for W-Sn
40 mineralization. A better understanding of the temporal and genetic association of the mineralization with the
41 spatially associated granitic batholith is an essential first step towards developing an effective strategy for
42 discovering potentially economic W-Sn deposits in this environment.

43 The Nanling region in the northwestern part of the Cathaysia block of the South China hosts more than
44 54% of the tungsten resources of the World as well as important resources of tin and rare metals (Lu, 1986;

45 USGS, 2017). Most of the deposits making up this resource are spatially associated with highly evolved
46 Mesozoic granitic stocks (Fig. 1). Numerous precise age determinations have shown that the tungsten, tin
47 and rare metal mineralization and the spatially-associated granitic intrusions are of Mesozoic age, and were
48 emplaced in three distinct episodes (Mao et al., 2013), namely a Late Triassic W-Sn-Nb-Ta episode
49 (Indosinian, 230-210 Ma; Cai et al. 2006; Yang et al. 2009), a Late Jurassic W-Sn episode (Early Yanshanian,
50 160-150 Ma, Peng et al. 2006, 2007; Jiang et al. 2008; Yuan et al. 2008a, 2011; Zhao et al. 2012; Hu et al.
51 2012a,b), and a Late Cretaceous Sn-Be-F episode (Late Yanshanian, ~90 Ma, Yuan et al. 2015).

52 In addition to the Mesozoic granites, there are also large granite batholiths of Caledonian age in the
53 Nanling region (Chen et al. 2013; Hua et al. 2013) (Fig. 2), which are second in importance volumetrically
54 only to the Yanshanian granites but have been thought to be unimportant from the perspective of W-Sn
55 mineralization. Recent successful exploration of the giant Zhangjialong tungsten deposit, however, is
56 changing this view (Hua et al. 2013). This deposit has proven WO_3 reserves of 57,300 t at a grade of 0.317%
57 WO_3 (Guo et al. 2017) and is located within the Penggongmiao granite batholith, which has been dated at
58 426.5 ± 2.5 Ma based on a LA-ICP-MS zircon U-Pb age for a scheelite-bearing aplitic dyke (Zhang et al.,
59 2011). As a result, a consensus is developing that there was also an important episode of tungsten
60 mineralization during the Caledonian (Qiao et al. 2011; Chen et al. 2013; Hua et al. 2013; Li et al. 2013), and
61 that the Caledonian granites and the adjacent pre-Silurian strata are favorable targets for regional W-
62 polymetallic mineralization (Qiao et al. 2011; Li et al. 2013; Guo et al., 2017). However, although the
63 Zhangjialong tungsten deposit is spatially associated with the Penggongmiao granite batholith, the age of the
64 mineralization has not been determined and thus a genetic association with the batholith has not been
65 established.

66 In this paper, we report results of systematic in-situ SIMS U-Pb, Ar-Ar and Re-Os dating of zircon,

67 muscovite and molybdenite, respectively, from greisen ore of the Zhangjialong tungsten deposit. Our new
68 geochronological data provide compelling evidence that the tungsten mineralization and greisenization of the
69 Zhangjialong deposit is of Late Jurassic, rather than Silurian age as previously thought. Our data therefore
70 preclude a temporal and genetic link between the tungsten mineralization and regional Caledonian
71 magmatism. Based on a regional geochronological data set, and a compilation of published whole-rock
72 geochemical data, we evaluate the potential of the granite batholiths for W-Sn mineralization from other
73 perspectives and in so doing advance our understanding of the W-Sn metallogenic potential of large granite
74 batholiths.

75

76 **2. Regional geological setting**

77 The Nanling region is located in the northwestern part of the Cathaysia block of South China (longitude
78 110°E-116°E, latitude 24°N-27°N), and covers a surface area of about 170,000 km². This region is
79 characterized by five separate granitic mountain ranges (the Yuechengling, Dupanling, Mengzhuling,
80 Qitianling and Dayuling), and is located at the junction of four provinces in southern China, namely Hunan;
81 Jiangxi; Guangdong; and Guangxi (Figs.1, 2) (Chen et al. 2002; Yuan et al. 2015). Previous age
82 determinations have shown that assembly of the Yangtze Craton and Cathaysia Block along the Qinhang
83 tectonic belt took place at ~1.1 to 0.83 Ga and coincided with the development of an Early Neoproterozoic
84 unconformity and the formation of the Jiangnan fold belt (e.g., Shui 1987; Chen and Jahn,1998; Zhao et al.
85 2011).

86 After assembly, the Nanling region in the central part of the South China Block was extensively
87 reworked during Caledonian, Indosinian, and Yanshanian tectonic-thermal events. These tectonic-thermal
88 events created a regional basement consisting of Sinian-Silurian clastic and metamorphic clastic rocks that

89 was overlain by a cover sequence of Devonian to Jurassic marine and marine-continental strata, including
90 carbonate rocks, marlstone and clastic beds (Mao et al, 2007). Between the Jurassic and Cretaceous, many
91 small fault-controlled depressions were filled by terrestrial clastic and volcanic rocks (Mao et al. 2007). In
92 addition, multiple episodes of granitic magmatism generated large volumes of granitic rocks in the Nanling
93 and neighboring regions (Mao et al. 2007; Hu and Zhou 2012), which are considered to have played an
94 important role in the W-Sn polymetallic pre-enrichment that culminated in large-scale Mesozoic W-Sn
95 mineralization (Hua et al. 2013).

96 The earliest granites are of Caledonian age and occur mainly as large batholiths along the boundaries of
97 Hunan, Jiangxi, Guangxi and Guangdong provinces (Fig. 2, Chen et al. 2013). These granites mainly belong
98 to the S-type class and formed in a regional Caledonian syn- or post-orogenic setting (Chen et al., 2013; Hua
99 et al., 2013; Ji et al., 2016). Until recently, they were not considered to be significant from the perspective of
100 W-Sn mineralization. Indosinian granitic magmatism in the Nanling region was triggered mainly by the
101 Indosinian orogeny and culminated in a series of post-collisional S-type granite batholiths (e.g., the Xitian
102 and Dengfuxian granite batholiths) or highly evolved granitic stocks (e.g., Limu; Zhou et al., 2003; Hua et
103 al., 2005). The Indosinian W-Sn mineralization in the Nanling region is mainly associated with highly
104 evolved Late Triassic post-collisional granitic stocks such as those hosting the Limu Sn deposit, the Liguifu
105 W-Sn deposit and the Shuiyuanshan and Yejiwo W deposits (Fig. 2, Yang et al., 2009; Zou et al., 2009; Mao
106 et al., 2013; Zhang et al., 2015). This was followed by large-scale Middle to Late Jurassic granitic magmatism
107 that was triggered by the westward subduction of the Paleo-Pacific Plate (Mao et al., 2013). The result was
108 the emplacement of large volumes of post-arc S-type or A-type granitic rocks and the formation of the largest
109 W-Sn metallogenic district in the World (Jiang et al., 2009; Mao et al., 2013; Chen et al., 2016) (Fig.2).

110 Most of the Middle to Late Jurassic W-Sn deposits are temporally, spatially, and genetically related to

111 highly evolved granitic stocks (Mao et al., 2007, 2013; Hu et al., 2012; Yuan et al., 2017). Recent exploration,
112 however, has revealed that a number of tungsten deposits or occurrences are located within Caledonian
113 granite batholiths or at their contacts zones. Examples of these deposits are the giant Zhangjialong tungsten
114 deposit and the smaller Zhenkou and Yangmeikeng tungsten deposits at the southern margin of the
115 Penggongmiao granite batholith (Lei et al, 2009; Li et al. 2013), the Yuntoujie, Jiepai, and Niutangjie
116 tungsten deposits at the southern margin of the Miao'ershan-Yuechengling granite batholith (Yang et al. 2014),
117 and the Liuyuan tin and the Zhuyuanli tungsten deposits within the Guidong granite batholith (Yuan et al.,
118 2018) (Fig. 2).

119

120 **3. Deposit geology**

121 The Zhangjialong ore deposit occurs at the southern margin of the Penggongmiao granite batholith
122 (975km²), which is located in eastern Hunan Province (Fig. 2). It comprises 46 orebodies, the largest nine of
123 which are mainly hosted in the granite batholith. The latter comprise disseminated and vein-style tungsten
124 mineralization in greisenized granite and provide much of the economic value of the deposit. They are
125 referred to hereafter as greisen-type orebodies. The five next most important orebodies comprise individual
126 quartz veins but are hosted within Sinian-Ordovician meta-sandstone intercalated with slate near the contact
127 with the batholith. The remaining ore bodies are of much less importance, occur as veins or disseminations
128 and are equally distributed between the granite and the host meta-sandstone. There are three sets of faults
129 developed in the area, with EW-, NW- and NE trends. Among these, the EW-trending faults are the dominant
130 regional structures and controlled the emplacement of the Penggongmiao granite batholith. The NW-trending
131 faults are well developed in the Zhangjialong area and cut the Penggongmiao granite batholiths. They formed
132 the main conduits for the fluids that altered the rocks and formed the tungsten orebodies (Figs. 4 and 5). The

133 NE-trending faults are the youngest and cut the Penggongmiao granite batholiths and the NW-trending faults.
134 Granitic magmatism in the Penggongmiao area occurred mainly between 447 and 426 Ma (Zhang et al.
135 2014). Based on detailed petrographic observations and zircon U-Pb dating, Zhang et al. (2014) divided the
136 Penggongmiao granite into two units, namely a fine-grained biotite granite with minor hornblende (G1 with
137 LA-ICP-MS zircon U-Pb ages of 447-442 Ma), and a medium- to coarse-grained porphyritic biotite
138 monzogranite (G2 with LA-ICP-MS zircon U-Pb ages of 436-431 Ma). The giant Zhangjialong W deposit is
139 hosted mainly in the G2 granite, and contains phenocrysts of K-feldspar and plagioclase in a groundmass of
140 K-feldspar, plagioclase, quartz and biotite (Fig. 6). Accessory minerals include apatite, rutile, titanite and
141 zircon (Zhang et al. 2011). In addition to the two main granitic units (G1 and G2), fine-grained scheelite-
142 bearing aplite dikes with a LA-ICP-MS zircon U-Pb age of 426.5 Ma occur locally (Zhang et al. 2011).

143 Hydrothermal alteration and mineralization were controlled mainly by NW-trending faults that cut the
144 medium- to coarse-grained porphyritic biotite monzogranite (G2) and Sinian clastic rocks (Figs. 4, 5).
145 Greisen is the dominant alteration associated with the tungsten mineralization (Fig.6) and developed mainly
146 in the medium- to coarse-grained porphyritic biotite monzogranite around the NW-trending faults (Figs. 4,
147 5). Silicification accompanied quartz vein-type tungsten mineralization developed along NW-trending faults
148 in the granite and Sinian clastic rocks (Figs.4, 5). As noted above, 46 separate orebodies have been discovered
149 in the Zhangjialong area. They represent a cumulative strike length of 100-3010 m, and width of 0.4-3.27 m
150 (1.38 m on average) and include the nine, main greisen-type orebodies and five main quartz-vein-type
151 orebodies mentioned above (Fig.4, Li et al. 2013; Guo et al., 2017). Among these, the No. 2 greisen-type
152 orebody is by far the largest one, with a strike length of 2320 m, and a width of 0.85-2.45 m. The most
153 common ore mineral of the greisen-type ore is scheelite (accounting for 90.5% of the tungsten resource in
154 this deposit) and is accompanied by minor amounts of molybdenite and pyrite. The main gangue and

155 alteration minerals are quartz and muscovite, which are intergrown with scheelite and molybdenite in the
156 greisen ore (Fig. 6). The most common ore mineral of the quartz-vein-type ore is scheelite, which is
157 accompanied by minor proportions of wolframite, molybdenite, bismuthinite, chalcopyrite, galena, sphalerite,
158 arsenopyrite and pyrite. The main gangue mineral is quartz, which occurs with small proportions of
159 muscovite; both are intergrown with scheelite, wolframite and molybdenite. Rocks hosting the vein-type
160 mineralization have been silicified for distances of 1-3 cm from the orebodies (individual veins).

161

162 **4. Sampling and analytical procedures**

163 The zircon used for U-Pb dating (Sample ZJL-2), molybdenite for Re-Os dating (Samples ZJL-5,6,7,8,9)
164 and the muscovite for Ar-Ar dating (Sample ZJL-2) were extracted from drill core containing greisenized
165 medium- to coarse-grained porphyritic biotite monzogranite and associated tungsten mineralization (Fig. 5).
166 The molybdenite is intergrown with muscovite and scheelite (Fig. 6). Zircon, muscovite and molybdenite
167 grains were separated using standard magnetic and heavy liquid techniques and were subsequently
168 handpicked under a binocular microscope at Chenxin Services Ltd., Langfang, China.

169 **4.1 Zircon SIMS U-Pb dating**

170 Representative zircon grains together with chips of the zircon standards, Plešovice and Qinghu, were
171 mounted in epoxy discs and polished to expose the longitudinal section of crystals for analysis. All zircon
172 crystals were examined in transmitted and reflected light, and with scanning electron microscopy (SEM), and
173 cathodoluminescence (CL) images were prepared to reveal their internal structures. The SEM was operated
174 with an accelerating voltage of 15 kV.

175 Measurements of U, Th and Pb isotope ratios were conducted using a Cameca IMS-1280HR SIMS at
176 the Institute of Geology and Geophysics, Chinese Academy of Sciences in Beijing. The analytical procedures

177 used during this study are similar to those described by Li et al. (2009), and only a brief summary is given
178 here. The primary O²⁻ ion beam spot is about 20×30 μm in area. Positive secondary ions were extracted with
179 a 10 kV potential. A 60 eV energy window was used in conjunction with a mass resolution of ca. 5400 (at
180 10% peak height) to separate Pb⁺ peaks from isobaric interferences. A single electron multiplier was used in
181 ion-counting mode to measure secondary ion beam intensities in peak jumping mode. Analyses of the zircon
182 standard, Plesovice, were alternated with analyses of unknown grains. Each measurement consisted of seven
183 cycles. The Pb/U calibration was performed relative to the zircon standard, Plesovice (²⁰⁶Pb/²³⁸U age = 337
184 Ma, Sláma et al. 2008); U and Th concentrations were calibrated against zircon standard 91500 (Th = 29
185 ppm, and U = 81 ppm, Wiedenbeck et al. 1995). A long-term uncertainty of 1.5% (1σ RSD) for ²⁰⁶Pb/²³⁸U
186 measurements of the standard zircon crystals was propagated to the unknowns (Li et al. 2010), although the
187 measured ²⁰⁶Pb/²³⁸U error in a specific session was generally ≤1% (1σ RSD). Measured compositions were
188 corrected for common Pb using non-radiogenic ²⁰⁴Pb. The corrections were sufficiently small to be
189 insensitive to the choice of a common Pb composition. An average present-day crustal composition (Stacey
190 and Kramers 1975) was used for the common Pb assuming that the latter was largely present due to surface
191 contamination during sample preparation. The data reduction was carried out using the Isoplot/Ex v. 2.49
192 program (Ludwig 2001). Uncertainties for individual analyses are reported at the 1σ level; Concordia U-Pb
193 ages are quoted with a 95% confidence interval, except where otherwise noted.

194 In order to monitor the external uncertainties associated with SIMS U-Pb zircon age determinations
195 calibrated against the Plesovice standard, an in-house zircon standard, Qinghu, was alternately analyzed as
196 an unknown with the other unknown zircon crystals. Twenty-two measurements of the Qinghu zircon yielded
197 a Concordia age of 160 ± 1 Ma, which is identical within error to the recommended value of 159.5 ± 0.2 Ma
198 (Li et al. 2013).

199 **4.2 Muscovite ^{40}Ar - ^{39}Ar dating**

200 The muscovite grains were sealed into a quartz bottle for irradiation in a nuclear reactor at the Chinese
201 Institute of Atomic Energy, Beijing; the total time for irradiation was 1444 min, the neutron flux was about
202 $2.60 \times 10^{13} \text{ n cm}^{-2}\text{S}^{-1}$, and the integrated neutron flux was $2.25 \times 10^{18} \text{ n cm}^{-2}$. The Fangshan biotite (ZBH-
203 25), with an age of $132.7 \pm 1.2 \text{ Ma}$ and a potassium content of 7.6%, was used as the internal standard. The
204 sample and monitors were heated in a graphite furnace after irradiation; the heating-extraction step for each
205 temperature increment was 30 minutes, with 20 minutes for purification. Mass analysis was carried out using
206 a Helix C Plus multiple collector noble gas mass spectrometer, and 20 sets of data were obtained for each
207 peak value. The analyses were performed in the Isotope Laboratory of the Institute of Geology, Chinese
208 Academy of Geosciences. The measured isotopic ratios were corrected for mass discrimination, atmospheric
209 Ar, blanks and irradiation-induced mass interference. The correction factors of interfering isotopes produced
210 during irradiation were determined by analysis of irradiated pure K_2SO_4 and CaF_2 , and yielded the following
211 ratios: $(^{36}\text{Ar}/^{37}\text{Ar})_{\text{Ca}} = 0.0002389$; $(^{40}\text{K}/^{39}\text{Ar})_{\text{K}} = 0.004782$; $(^{39}\text{Ar}/^{37}\text{Ar})_{\text{Ca}} = 0.000806$. Lambda, the decay
212 constant, was taken to be $5.543 \times 10^{-10} \text{ year}^{-1}$ (Steiger and Jager, 1977) and all ^{37}Ar abundances were
213 corrected for radiogenic decay (half-life 35.1 days). The plateau age, and the isochron and inverse isochron
214 were calculated using the ISOPLOT program (Ludwig, 2003); the uncertainties in the ages are reported at
215 the 95% confidence level (2σ). Details of the operating and data processing procedures were described by
216 Chen et al. (2006).

217 **4.3 Molybdenite Re-Os dating**

218 Molybdenite Re-Os isotopic analyses were performed using a Thermo Electron TJA X-series ICP-MS
219 instrument in the Re-Os laboratory at the National Research Center of Geoanalysis, Chinese Academy of
220 Geosciences, Beijing, China. The analytical procedures used during this study were similar to those described

221 by Du et al. (2009), Mao et al. (1999) and Stein et al. (2001). The Re-Os model ages were calculated using
222 $t = [\ln(1 + {}^{187}\text{Os}/{}^{187}\text{Re})] / \lambda$, where λ is the decay constant of ${}^{187}\text{Re}$ of $1.666 \times 10^{-11} \text{ year}^{-1}$ (Smoliar et al. 1996).
223 The Re-Os isochron age was calculated using the ISOPLOT 2.49 program (Ludwig 2001). The uncertainty
224 in the Re-Os model ages includes a 1.02% uncertainty in the ${}^{187}\text{Re}$ decay constant, an uncertainty in the spike
225 calibration, and the mass spectrometry analytical error (Du et al., 2009).

226 **5. Results**

227 **5.1. SIMS Zircon U-Pb age**

228 Spot analyses were conducted on 28 zircon grains in sample ZJL-2 from greisenized granite associated
229 with tungsten mineralization using in situ SIMS U-Pb. The zircon grains and grain fragments are generally
230 colorless, transparent, euhedral, and range between 50 and 250 μm in length with length/width ratios of 1- 4.
231 In CL images, most of the zircon crystals show evidence of oscillatory zoning with fine bands
232 (Supplementary Fig. 1). Together, these features indicate that the zircon is of magmatic origin (Hoskin and
233 Schaltegger 2003). Results of in-situ zircon U-Th-Pb analyses on domains showing oscillatory zoning are
234 presented in Supplementary Table 1. Zircon crystals from sample ZJL-2 have U contents and Th/U ratios
235 varying from 202 ppm to 1751 ppm and from 0.23 to 0.53 (Supplementary Table 1), respectively. All the data
236 from the 28 analyses are concordant and yield a Concordia age of $441.3 \pm 2.4 \text{ Ma}$ (MSWD=0.043) (Fig. 7a),
237 which is the best estimate of the crystallization age of sample ZJL-2. Our new SIMS U-Pb age for the
238 greisenized granite is indistinguishable within error from previously published LA-ICP-MS U-Pb zircon ages
239 of $436.2 \pm 3.1 \text{ Ma}$ to $435.3 \pm 2.7 \text{ Ma}$ for the medium coarse-grained biotite granite and is significantly older
240 than the LA-ICP-MS U-Pb zircon age of $426.5 \pm 2.5 \text{ Ma}$ for the aplitic dykes crosscutting the porphyritic
241 biotite granite (Zhang et al. 2011).

242 **5.2 Muscovite Ar-Ar dating**

243 ^{40}Ar - ^{39}Ar age determinations were carried out on muscovite grains intergrown with scheelite and
244 molybdenite from the greisen-type ore (separate ZJL-2); the analytical results are listed in Supplementary
245 Table 2, and illustrated in Figure 8. The apparent ages obtained from the low-temperature steps are not
246 considered to have geological significance because of the low percentage of $^{39}\text{Ar}_k$ released (Yuan et al. 2007,
247 2010, 2015), which was likely caused by the initial loss of small quantities of Ar from the edges of mineral
248 grains (Hanson et al. 1975). In contrast, the eleven continuous steps at temperatures of 770-1400 °C are
249 almost coincident and constitute a uniform and remarkably flat $^{40}\text{Ar}/^{39}\text{Ar}$ age spectrum with 99.35% $^{39}\text{Ar}_k$
250 released. These steps yield a well-defined plateau age of 153.5 ± 1.0 Ma (MSWD=1.2), an isochron age of
251 153.0 ± 1.5 Ma (MSWD = 3.1) for an initial $^{40}\text{Ar}/^{36}\text{Ar}$ ratio of 300.6 ± 5.8 , and an inverse isochron age of
252 152.9 ± 1.5 Ma (MSWD = 6.4) for an initial $^{40}\text{Ar}/^{36}\text{Ar}$ ratio of 301.9 ± 5.3 (MSWD = 6.4) (Fig. 8). The
253 agreement among the plateau age, the isochron age and the inverse isochron age is excellent, and within the
254 applicable analytical uncertainty. The plateau age (153.5 ± 1.0 Ma) is considered to represent the best estimate
255 of the crystallization age of the muscovite.

256

257 **5.3 Molybdenite Re-Os dating**

258 The Re and Os abundances and isotopic data for the molybdenite samples are listed in Supplementary
259 Table 3. Total Re and ^{187}Os concentrations vary from 1665 ng/g to 2135ng/g, and from 2.821 ng/g to 3.535
260 ng/g (Supplementary Table 3), respectively. The Re-Os model ages of the five molybdenite samples range
261 from 157.9 ± 2.3 Ma to 161.7 ± 2.4 Ma with a weighted mean of 160.4 ± 2.2 Ma (MSWD=2.2). The isochron
262 age for all five samples is 150 ± 25 Ma with a MSWD of 3.9 (Fig. 7b). Considering that the Re-Os model
263 ages vary in a relatively narrow range and the error of the weighted mean age (MSWD=2.2) is smaller than
264 that of the isochron age (MSWD=3.9), the weighted mean of 160.4 ± 2.2 Ma is interpreted as the age of

265 molybdenite crystallization in the Zhangjialong W deposit.

266

267 **6. Discussion**

268 **6.1 Timing of granite emplacement and tungsten mineralization**

269 Zhang et al. (2011) reported zircon LA-ICP-MS U-Pb ages for the biotite granite and a scheelite-bearing
270 aplitic dyke cross-cutting the granite of 436-435 Ma and 426.5 ± 2.5 Ma, respectively. Because of this and the
271 fact that that the Zhangjialong tungsten deposit is mainly hosted by the Penggongmiao granite batholith, most
272 researchers have taken this deposit to be an example of tungsten mineralization genetically related to
273 Caledonian granite magmatism (Qiao et al. 2011; Chen et al. 2013; Li et al. 2013). Our direct Re-Os dating
274 of molybdenite, however, has provided a precise age of 160.4 ± 2.2 Ma for the quartz-vein-hosted
275 mineralization, which is broadly consistent with the ^{40}Ar - ^{39}Ar plateau age (153.5 ± 1.0 Ma) of muscovite
276 intergrown with scheelite in the greisen and considerably younger than the zircon SIMS U-Pb age of 441.3
277 ± 2.4 Ma for greisenized granite that hosts the ore. This shows clearly that the hydrothermal tungsten
278 mineralization is temporally and genetically unrelated to Caledonian granite magmatism.

279 Our new molybdenite Re-Os age (160.4 ± 2.2 Ma) and muscovite Ar-Ar age (153.5 ± 1.0 Ma) are well
280 within the range of those for Late Jurassic W-Sn deposits (160-150 Ma) in the Nanling region (Yuan et al.
281 2007, 2008a, 2012a, b; Peng et al. 2006, 2007; Hu et al. 2012a, b; Hu and Zhou, 2012; Mao et al. 2004, 2007,
282 2013). Accordingly, we propose that the tungsten mineralization of the Zhangjialong deposit was introduced
283 by hydrothermal fluids associated with a concealed Late Jurassic granite pluton. Late Jurassic granite
284 magmatism therefore satisfactorily explains the tungsten mineralization of the Zhangjialong area, and thus
285 any exploration of the Penggaomian batholith for tungsten based on a model involving a genetic relationship
286 between this mineralization and Caledonian magmatism is fundamentally flawed.

287

288 **6.2 Genesis of the W-Sn deposits hosted within large granite batholiths**

289 As mentioned in the introduction to this paper, most W-Sn deposits typically occur in close proximity to
290 differentiated granites. This also applies to the Nanling region, where most of the giant W-Sn deposits are
291 spatially associated with small, highly evolved granitic Mesozoic granite stocks (ca.160-150 Ma; Fig. 2) with
292 which they are considered to be genetically related (Mao et al. 2004; Yuan et al., 2008b, 2011, 2015; Liu et
293 al. 2012).

294 However, mineral exploration during the past few years has shown that, in addition to the Zhangjialong W
295 deposit, several other large W and W-Sn deposits occur within or near Caledonian granite batholiths. For
296 example, in the western part of the Nanling region, the Niutangjie, Jiepai and Gaoling W deposits and the
297 Yuntoujie W-Mo deposit are distributed along the southern and eastern margin of the Miaoershan (MES)-
298 Yuechengling (YCL) granite batholith (with an exposure area of about 3000 km²) (Fig. 2). Significantly,
299 however, the Niutangjie W deposit has been shown recently to be genetically related to a highly evolved
300 Caledonian granite stock rather than the batholith (Yang et al., 2014). The spatial association with Caledonian
301 granitic batholiths also applies to the Liguifu W-Sn and the Limu Sn deposits, which are located within the
302 eastern and southeastern margin of the Haiyangshan (HYS)-Dupangling (DPL) granite batholith (with an
303 exposure area of about 650 km²) (Fig. 2).

304 The above association extends to the Mesozoic batholiths. Thus, for example, the giant Xitian tin deposit
305 in southern Hunan Province is located within the Indosinian (230-210 Ma) Xitian granite batholith (with an
306 exposure area of about 240 km²) near its contact with Devonian dolomitic limestone (Fig. 2). This is also true
307 for the nearby large Dengfuxian tungsten deposit, which occurs within the Indosinian Dengfuxian granite
308 batholith (with an exposure area of about 170 km²) (Fig. 2). High precision zircon U-Pb, molybdenite Re-Os

309 and muscovite Ar-Ar data now show, however, that both the Xitian Sn and Dengfuxian W deposits formed at
310 160-150 Ma, and are genetically related to highly evolved Late Jurassic (Early Yanshanian) granite stocks
311 (Liu et al. 2008; Ma et al. 2008; Fu et al. 2009; Guo et al. 2014; Cai et al. 2012; Huang et al. 2013; Liang et
312 al. 2016) rather than the Indosinian granite batholiths (Cai et al., 2013; Liu et al. 2015).

313 In other parts of the World, notably the Southeast Asian Sn belt, the Central Portuguese W-Sn district, the
314 Erzgebirge tin province in Germany and the Blue Tier tin district in Australia, W-Sn deposits also occur
315 commonly within or adjacent to granite batholiths. Most of these deposits, however, are genetically related
316 to highly evolved younger granite stocks or cupolas (Durisova et al., 1979; Föster et al., 1999; Yokart et al.,
317 2003; Webster et al., 2004).

318

319 **6.3 The W-Sn metallogenic potential of large granite batholiths**

320 Tin and tungsten are present in higher concentrations in reduced ilmenite-series S-type granitic magmas
321 than other granitic magmas and, owing to their incompatibility, accumulate in the residual liquid during
322 magmatic differentiation (Ishihara et al., 1979). Consequently, advanced magmatic fractionation has been
323 considered a key criterion for identifying S-type granites that might host genetically related Sn-W deposits
324 (Lehmann 1982, 1987, 1990; Lehmann and Mahawat 1989). For the same reason, the granites are thought to
325 be more likely to occur as small stocks rather than larger intrusions.

326 In order to further evaluate the hypothesis that economic W-Sn mineralization in granite batholiths is
327 genetically related to small, highly evolved stocks that intrude these batholiths, we have compiled the
328 available whole-rock geochemical data for the granitic rocks that form the batholiths and the W-Sn-bearing
329 granite stocks in the Nanling region (Figs. 1, 2, Supplementary Table 4). These data show that the large
330 granite batholiths in the region (such as the Miao'eshan, Yuechengling, Haiyangshan, Dupangling,

331 Dengfuxian, Xitian, Penggaomiao and Wanyangshan granite batholiths) are less differentiated than W-Sn-
332 bearing granite stocks such as the Qianlishan (QLS), the Laiziling (LZL), the Jiangfengling (JFL), and
333 Xihuashan (XHS) stocks (Figs. 9, 10; Yao et al. 2005; Cheng et al. 2012, 2013; Xuan et al. 2014; Chen et al.
334 2014). The granites of the stocks can be distinguished from those of the batholiths by their chondrite-
335 normalized REE profiles and their Rb/Sr, K/Rb, Nb/Ta, Zr/Hf ratios (Fig. 9 and 10). Thus, the granite stocks
336 are characterized by flat to moderate heavy REE enrichment, whereas the granites of the batholiths display
337 heavy REE depletion (Fig. 9). Similarly, the granitic stocks have high Rb/Sr ratios (>9), and low Nb/Ta ratio
338 (<5), Zr/Hf ratio (<20) and K/Rb ratio (<60), whereas the opposite is the case for the granitic batholiths (Fig.
339 10; Soloviev 2011, 2014; Ballouard et al. 2016). Most significantly, and consistent with the incompatibility
340 of W and Sn, the concentrations of these elements in the granitic stocks range from 23 to 51 ppm, which
341 contrasts strongly with those of the granitic batholiths that are in the range 1.2 to 21 ppm (Cheng et al., 2013).

342 In view of the much higher W and Sn contents of the evolved stocks relative to their batholithic parents, it
343 is reasonable to predict that the granites of the stocks are more likely to be the source of economic W-Sn
344 mineralization than those of the batholiths. An additional and potentially more important reason for the stocks
345 being the source of the metals is that the granite batholiths are emplaced at mid-crustal levels and thus
346 relatively high pressure. Consequently, there is limited development of hydraulic fracturing and the release
347 of magmatic hydrothermal fluids is unfocused, both of which are unfavorable for the formation of economic
348 deposits. In contrast, small, highly evolved stocks represent cupolas that develop kilometers above the general
349 level of emplacement of the batholiths. As such, they are emplaced at shallow crustal levels where hydraulic
350 fracturing is intense and the release of hydrothermal fluids from the magma is highly focused. This, and the
351 convective magma overturn that ensures the introduction of multiple batches of H₂O-rich magma into the
352 cupolas, facilitating the large-scale hydrothermal alteration and, in principle, the multi-stage W-Sn rare metal

353 mineralization that are the signatures of economic W-Sn deposits.

354 **6.4 Differential competence as a control of W-Sn mineralization in granite batholiths**

355 Although, as discussed above, granite batholiths are not predicted to produce W-Sn deposits directly, the
356 occurrence of economic deposits within, albeit close to their margins, suggests that this spatial association is
357 more than coincidence. We propose that the reason for this association in the Nanling region is that, because
358 there is a large difference in the competence of the granite and the adjacent metasedimentary rocks, fractures
359 developed preferentially along the contacts between the two rock-types in response to tectonic events, and
360 these fractures provided the conduits for the subsequent emplacement of later granitic stocks. As the
361 Caledonian granites occur mainly in the form of large batholiths, we further propose that most of the higher
362 level Caledonian stocks have been eroded and that the Caledonian W-Sn mineralization is now of minor
363 importance. However, because late Mesozoic magmatism, corresponding to the Yanshanian event, produced
364 large volumes of evolved granitic magma that could be emplaced along fractures immediately adjacent to
365 older batholiths of Caledonian and Indosinian age (after considerable erosion of these batholiths), there is
366 now a strong spatial association between the batholiths and economic W-Sn mineralization. Thus, although
367 Caledonian batholiths were not the source of the economic W-Sn mineralization exemplified in the
368 Zhangjialong W deposit, their contacts represent very favourable locations for the discovery of new economic
369 W-Sn deposits.

370

371 **7. Conclusions**

372 A combination of Re-Os dating of molybdenite and Ar-Ar dating of muscovite intergrown with scheelite
373 and molybenite shows that the Zhangjialong W deposit formed during the Yanshanian event, i.e., between
374 160 and 150 Ma, whereas SIMS U-Pb dating of zircon (441.3 ± 2.4 Ma) in the greisenized granite confirms

375 that the latter is of Caledonian age. This precludes a temporal and genetic link between hydrothermal tungsten
376 mineralization and the regional Caledonian granite magmatism. Instead, the geochronological data and
377 evidence that granitic stocks are more evolved and more enriched in W and Sn suggests strongly that the
378 latter are the source of the W-Sn mineralization in these and the younger Indosinian batholiths. We propose
379 1) that the W-Sn mineralization, which is spatially associated with the batholiths originated from younger
380 stocks emplaced at high crustal levels, thereby enabling focused release of W-Sn enriched hydrothermal
381 fluids, and 2) that the location of the deposits near the margins of the batholiths was a result of differential
382 competence between the granites and the host metasedimentary rocks, which facilitated tectonic-induced
383 fracturing and emplacement of the magmas that produced W-Sn fertile stocks.

384 **Acknowledgments**

385 This research was financially supported by the National Key Research and Development Project of China
386 (No.2016YFC0600205), the National Nonprofit Institute Research Grant of CAGS (YYWF201711), and the
387 National Natural Science Foundation of China (Nos. 41373047, 41672095). We express our gratitude to Prof.
388 Bernd Lehmann for his suggestions that helped improve an early draft of this paper.

389 **References**

- 390 Ballouard C, Poujol M, Boulvais P, Branquet Y, Tartèse R, Vigneresse J-L (2016) Nb-Ta fractionation in
391 peraluminous granites: A marker of the magmatic-hydrothermal transition. *Geology* 44: 231-234
- 392 Bo DY, Huang JZ, Ma TQ, Wang XH (2006) Geology and geochemistry of the silurian penggongmiao
393 granitic pluton in the southeastern Hunan Province and its implication for tectonic setting. *Geoscience*
394 20:130-140 (in Chinese with English abstract)
- 395 Cai MH, Chen KX, Qu WJ, Liu GQ, Fu JM, Yin JP (2006) Geological characteristics and Re-Os dating of
396 molybdenites in Hehuaping tin-polymetallic deposit, southern Hunan Province. *Mineral Deposits*

- 397 25:263-268 (in Chinese with English abstract)
- 398 Cai Y, Lu JJ, Ma DS, Huang H, Zhang HF (2013) Chronology and geochemical characteristics of Late
399 Indosinian Dengfuxian two-mica granite in eastern Hunan Province, China, and its significance. *Acta*
400 *Petrologica Sinica* 29:4215-4231(in Chinese with English Abstract)
- 401 Cai Y, Ma DS, Lu JJ, Huang H, Zhang RQ, Qu WJ (2012) Re-Os geochronology and S isotope geochemistry
402 of Dengfuxian tungsten deposit, Hunan Province, China. *Acta Petrol Sin* 28:3798-3808(in Chinese with
403 English Abstract)
- 404 Černý P, Blevin PL, Cuney M, London D (2005) Granite-related ore deposits. In *Economic Geology One*
405 *Hundredth Anniversary Volume* (eds. Hedenquist JW, Thompson JFH, Goldfarb RJ and Richards RJ).
406 337-370
- 407 Chen D, Shao YJ, Liu W, Ma AJ, Liu YR (2014) Petrological characteristics of Xitian pluton in Hunan
408 province. *Geol Miner Resour South China* 31:11-25(in Chinese with English Abstract)
- 409 Chen J, Wang RC, Zhu JC, Lu JJ, Ma DS (2013) Multiple-aged granitoids and related tungsten-tin
410 mineralization in the Nanling Range, South China. *Science China Earth Sciences* 56:2045-2055
- 411 Chen MH, Mo CS, Huang ZZ, Li B, Huang HW (2011) Zircon LA-ICP-MS U-Pb ages of granitoid rocks
412 and molybdenite Re-Os age of Shedong W-Mo deposit in Cangwu County of Guangxi and its geological
413 significance. *Mineral Deposits* 30: 963-978(in Chinese with English abstract)
- 414 Chen PR, Hua RM, Zhang BT, Lu JJ, Fan CF (2002) Early Yanshanian post-orogenic granitoids in the
415 Nanling region-petrological constraints and geodynamic settings. *Sci China* 45: 755-768
- 416 Cheng SB, Fu JM, Cheng XQ, Ma LY, Lu YY (2012) Zircon SHRIMP U-Pb dating and geochemical
417 characteristics of Haiyangshan monzogranitic batholiths, northeast Guangxi. *Geology and Mineral*
418 *Resources of South China* 28: 132-140 (in Chinese with English abstract)

- 419 Cheng SB, Fu JM, Ma LY, Jian GX, Chen XQ, Lu YY, Tong XR (2013) Indosinian metallogenic activity in
420 Yuechengling-Miaoershan area, northeastern Guangxi: implications from zircon U-Pb ages and Hf
421 isotopic constraint on ore-forming granites in Youmaling and Jiepai deposits. *Geology in China* 40:
422 1189-1201(in Chinese with English Abstract)
- 423 Förster HJ, Romer RL, Gottesmann B, Tischendorf G, Rhede D (2009) Are the granites of the Aue-
424 Schwarzenberg zone (Erzgebirge, Germany) a major source for metalliferous ore deposits? A
425 geochemical, Sr-Nd-Pb isotopic, and geochronological study. *N Jb Miner Abh* 186: 163-184
- 426 Fu JM, Wu SC, Xu DM, Ma LY, Cheng SB, Chen XQ (2009) Reconstraint from zircon SHRIMP U-Pb dating
427 on the age of magma intrusion and mineralization in Xitian tungsten-tin polymetallic orefield, eastern
428 Hunan Province. *Geol Miner Resour South China* 37:1-7(in Chinese with English Abstract)
- 429 Guo C. L., Li C., Wu S. C. & Xu Y. M. (2014) Molybdenite Re-Os isotopic dating of Xitian deposit in Hunan
430 Province and its geological significance. *Rock Miner Anal* 33:142-152 (in Chinese with English
431 Abstract)
- 432 Guo CL, Chen YC, Zeng ZL, Lou FS (2012) Petrogenesis of the Xihuashan granites in southeastern China:
433 Constraints from geochemistry and in-situ analyses of zircon U – Pb – Hf – O isotopes. *Lithos* 148:209
434 – 227
- 435 Guo CL, Wang RC, Yuan SD, Wu SH, Yin B (2015) Geochronological and geochemical constraints on the
436 petrogenesis and geodynamic setting of the Qianlishan granitic pluton, Southeast China. *Miner Petrol*
437 109: 253 – 282
- 438 Hu RZ, Wei WF, Bi XW, Peng JT, Qi YQ, Wu LY, Chen YW (2012b) Molybdenite Re-Os and muscovite
439 $^{40}\text{Ar}/^{39}\text{Ar}$ dating of the Xihuashan tungsten deposit, central Nanling district, South China. *Lithos*
440 150:111-118

- 441 Hu R Z, Zhou MF (2012) Multiple Mesozoic mineralization events in South China—an introduction to the
442 thematic issue. *Mineralium Deposita* 47:579-588.
- 443 Hu RZ, Bi XW, Jiang GH, Chen HW, Peng JT, Qi YQ, Wei WF (2012c) Mantle-derived noble gases in ore-
444 forming fluids of the granite-related Yaogangxian tungsten deposit, Southeastern China. *Mineralium*
445 *Deposita* 47:623-632
- 446 Hu RZ, Wei WF, Bi XW, Peng JT, Qi YQ, Wu LY, Chen YW (2012a) Molybdenite Re–Os and muscovite ⁴⁰
447 Ar/³⁹Ar dating of the Xihuashan tungsten deposit, central Nanling district, South China. *Lithos* 150:111-
448 118
- 449 Hua RM, Zhang WL, Chen PR, Zhai W, Li GL (2013) Relationship between Caledonian granitoids and large-
450 scale mineralization in South China. *Geological Journal of China Universities* 19:1-11 (in Chinese with
451 English abstract)
- 452 Huang H, Ma DS, Lu JJ, Cai Y, Xie X (2013) Zircon U-Pb geochronology and geochemistry characteristics
453 of Dengfuxian two-mica granite, eastern Hunan Province, China. *Acta Mineralogica Sinica* 33:245-
454 255(in Chinese with English Abstract)
- 455 Hulsbosch N, Boiron MC, Dewaele S, Muchez P (2016) Fluid fractionation of tungsten during granite-
456 pegmatite differentiation and the metal source of peribatholithic W quartz veins: Evidence from the
457 Karagwe-Ankole Belt (Rwanda). *Geochimica et Cosmochimica Acta* 175: 299-318
- 458 Jiang SY, Zhao KD, Jiang YH, Dai BZ (2008) Characteristics and genesis of Mesozoic A-type granites and
459 associated mineral deposits in the southern Hunan and northern Guangxi provinces along the Shi-Hang
460 belt, South China. *Geological Journal of China Universities* 14: 496-509 (in Chinese with English
461 Abstract)
- 462 Lehmann B, Mahawat C (1989) Metallogeny of tin in central Thailand: A genetic concept. *Geology* 17:426-

- 463 429
- 464 Lehmann B (1982) Metallogeny of tin; magmatic differentiation versus geochemical heritage. *Economic*
465 *Geology* 77: 50-59
- 466 Lehmann B (1987) Tin granites, geochemical heritage, magmatic differentiation. *Geologische Rundschau* 76:
467 177-185
- 468 Lehmann B (1990) *Metallogeny of tin*. Springer, v 32.
- 469 Lei ZH, Xu YM, Wang DH, Qiao YS, Li CB, Chen ZH (2009) Metallogenic geological conditions and
470 tungsten-polymetallic ore prospecting in Guidong-Rucheng area, Hunan Province. *Acta Geosciencia*
471 *Sinica* 30: 812-820 (in Chinese with English Abstract)
- 472 Li HY, Mao JW, Sun YL, Zou XQ, He HL, Du AD (1996) Re-Os isotopic chronology of molybdenites in
473 the Shizhuyuan polymetallic tungsten deposit, southern Hunan. *Geological Review* 42:261-267 (in
474 Chinese with English Abstract)
- 475 Li SQ, Lan XM, Deng SH, Chen SF, Wang FY, Li CB, Huang GH (2013) Metallogenic geological
476 characteristics of Caledonian tungsten deposits in Zhenkou area of Hunan Province and ore-prospecting
477 orientation. *Mineral Deposits* 32:405-414 (in Chinese with English Abstract)
- 478 Li WJ, Liang JC, Feng ZH, Zhang GL, Chen MH, Yuan AP (2006) Judging for characterstics of geochemical
479 and structural environment of several Caledonian granitoids in northeast Guangxi. *Mineral Resources*
480 *and Geology* 20:353 – 356 (in Chinese with English abstract)
- 481 Li XF, Feng ZH, Li RS, Tang ZH, Qu WJ, Li JC (2009) Silurian Mo mineralization at Baishiding
482 molybdenum deposit in northern Guangxi: Constraints from zircon SHRIMP U-Pb and molybdenite Re-
483 Os ages. *Mineral Deposits* 28:403-412 (in Chinese with English abstract)
- 484 Liang XQ, Dong CG, Jiang Y, Wu SC, Zhou Y, Zhu HF, Fu JG, Wang C, Shan YH (2016) Zircon U-Pb,

485 molybdenite Re-Os and muscovite Ar-Ar isotopic dating of the Xitian W-Sn polymetallic deposit,
486 eastern Hunan Province, South China and its geological significance. *Ore Geology Reviews* 78:85-100

487 Liu GQ, Wu SC, Du AD, Fu JM, Yang XJ, Tang ZH, Wei JQ (2008) Metallogenic ages of the Xitian tungsten-
488 tin deposit, eastern Hunan province. *Geotecton. Metallog* 32:63-71(in Chinese with English Abstract)

489 Liu XF, Yuan SD, Wu SH (2012) Re-Os dating of the molybdenite from the Jinchuantang tin-bismuth deposit
490 in Hunan Province and its geological significance. *Acta Petrologica Sinica* 28:39-51(in Chinese with
491 English Abstract)

492 Lu HZ (1986) Origin of tungsten mineral deposit in South China (in Chinese with English Abstract).
493 Publishing House of Chongqing, pp1-232

494 Ma TQ, Bai DY, Kuang J, Wang XH (2005) Zircon SHRIMP dating of the Xitian granite pluton, Chaling,
495 southeastern Hunan, and its geological significance. *Geol. Bull. China* 24:415-419 (in Chinese with
496 English Abstract)

497 Mao JW, Cheng YB, Chen MH, Franco Pirajno (2013) Major types and time-space distribution of Mesozoic
498 ore deposits in South China and their geodynamic settings. *Mineralium Deposita* 48: 267-294

499 Mao JW, Li XF, Chen W, Lan XM, Wei SL (2004) Geological characteristics of the Furong tin orefield,
500 Hunan, ^{40}Ar - ^{39}Ar dating of tin ores and related granite and its geodynamic significance for rock and ore
501 formation. *Acta Geologica Sinica (English Edition)* 78: 481-491

502 Mao JW, Xie GQ, Guo CL (2007) Large-scale tungsten-tin mineralization in the Nanling region, South China:
503 metallogenic ages and corresponding geodynamic processes. *Acta Petrol. Sin* 23:2329-2338 (in Chinese
504 with English Abstract)

505 Mao JW, Xie GQ, Guo CL, Yuan SD, Cheng YB, Chen YC (2008) Spatial-temporal distribution of Mesozoic
506 ore deposits in South China and their metallogenic setting. *Geological Journal of China Universities*

507 14:510-526 (in Chinese with English Abstract)

508 Mao JW, Zhou ZH, Feng CY, Wang YT, Zhang CQ, Peng HJ, Yu M (2012) A preliminary study of the Triassic
509 large-scale mineralization in China and its geodynamic setting. *Geology in China* 39:1437-1471 (in
510 Chinese with English Abstract)

511 Niu R, Liu Q, Hou QL, Sun JF, Wu SC, Zhang HY, Guo QQ, Wang Q (2015) Zircon U-Pb geochronology of
512 Xitian granitic pluton in Hunan Province and its constraints on the metallogenic ages of the tungsten-
513 tin deposit. *Acta Petrologica Sinica* 31:2620-2632(in Chinese with English Abstract)

514 Peng JT, Hu RZ, Bi XW, Dai TM, Li ZL, Li XM, Shuang Y, Yuan SD, Liu SR (2007) $^{40}\text{Ar}/^{39}\text{Ar}$ isotopic
515 dating of tin mineralization in Furong deposit of Hunan Province and its geological significance. *Mineral
516 Deposits* 26:237-248 (in Chinese with English abstract)

517 Peng JT, Zhou MF, Hu RZ, Shen NP, Yuan SD, Bi XW, Du AD, Qu WJ (2006) Precise molybdenite Re-Os
518 and mica Ar-Ar dating of the Mesozoic Yaogangxian tungsten deposit, central Nanling district, South
519 China. *Mineralium Deposita* 41:661-669

520 Pitakpaivan K (1969) Tin bearing granite and tin barren granite in Thailand. In: Second Technical Conference
521 on Tin, Bangkok, Thailand, 1, 283-298.

522 Qiao YS, Wang FY, Hou MS, Lei ZH, Li CB (2011) Geological characteristics of Zhangjialong tungsten
523 deposit, Hunan Province. *Geology and Mineral Resources of South China* 27:125-131 (in Chinese with
524 English Abstract)

525 Soloviev S (2011) Geology, mineralization, and fluid inclusion characteristics of the Kensu W-Mo skarn and
526 Mo-W-Cu-Au alkalic porphyry deposit, Tien Shan, Kyrgyzstan. *Economic Geology* 106: 193-222.

527 Soloviev S (2014) Geology, mineralization, and fluid inclusion characteristics of the Kumbel oxidized W-
528 Cu-Mo skarn and Au-W stockwork deposit in Kyrgyzstan, Tien Shan. *Mineralium Deposita* 50: 187-

- 529 220.
- 530 Taylor RG (1979) Geology of tin deposits. *Developments in Economic Geology*, pp 11
- 531 USGS (2017) U.S. Geological Survey Mineral Commodity Summaries. Tungsten, pp 180-181
- 532 Wang XG, Zhu JC (1992) Origin, evolution and prospecting significance of granites in the Gejiu tin field,
533 Yunnan Province. *Geotectonica Et Metallogenia* 4:009 (in Chinese with English abstract)
- 534 Wilkinson JJ (1990) The role of metamorphic fluids in the development of the Cornubian orefield: fluid
535 inclusion evidence from south Cornwall. *Mineralogical Magazine* 54:219-230
- 536 Wu GY, Ma TQ, Feng YF, Yan QR, Liu FG, Bo DY (2008) Geological and geochemical characteristics and
537 genesis of the Caledonian Wanyangshan granite in the Nanling Mountains, South China. *Geology in*
538 *China* 35: 608 – 617 (in Chinese with English abstract)
- 539 Wu J, Liang HY, Huang WT, Wang CL, Sun WD, Sun YL, Li J, Mo JH, Wang XZ (2012) Indosinian isotope
540 ages of plutons and deposits in southwestern Miaoshan-Yuechengling, northeastern Guangxi and
541 implications on Indosinian mineralization in South China. *Chinese Science Bulletin* 57:1024-1035
- 542 Wu SC, Hong QH, Long WP, Luo Y (2009) Geological features and metallogenic model of Xitian W-Sn
543 polymetallic deposit, Hunan Province. *Geology and Mineral Resources of South China* 2:1-6 (in
544 Chinese with English Abstract)
- 545 Xu DM, Fu JM, Chen XQ, Cheng SB, Ma LY, Zhang K, Huang H (2017) Formation age and petrogenesis of
546 the Dupangling rapakivi granites and its geological significance. *Geotectonica et Metallogenia*, 41: 561-
547 576 (in Chinese with English abstract)
- 548 Xuan YS, Yuan SD, Yuan YB, Mi JR (2014) Zircon U-Pb age, geochemistry and petrogenesis of Jianfengling
549 pluton in southern Hunan Province. *Mineral Deposits* 33:1379-1390 (in Chinese with English abstract)
- 550 Yang F, Li XF, Feng ZH, Bai YP (2009) $^{40}\text{Ar}/^{39}\text{Ar}$ dating of muscovite from greisenized granite and

551 geological significance in Limu tin deposit. *J. Guilin Univ. Technol* 29:21-24 (in Chinese with English
552 abstract)

553 Yang F, Li XF, Feng ZH, Bai YP (2009) $^{40}\text{Ar}/^{39}\text{Ar}$ dating of muscovite from greisenized granite and
554 geological significance in Limu tin deposit. *Journal of Guilin University of Technology* 29: 21-24 (in
555 Chinese with English abstract)

556 Yang Z, Wang RC, Zhang WL, Chu ZY, Chen J, Zhu JC, Zhang RQ (2014) Skarn-type tungsten
557 mineralization associated with the Caledonian (Silurian) Niutangjie granite, northern Guangxi, China.
558 *Science China Earth Sciences* 57:1551-1566

559 Yao JM, Hua RM, Lin JF (2005) Zircon LA-ICPMS U-Pb dating and geochemical characteristics of the
560 Huangshaping granite in southeast Hunan province, China. *Acta Petrologica Sinica* 21:688-696(in
561 Chinese with English abstract)

562 Yokart B, Barr SM, Williams-Jones AE, Macdonald AS (2003) Late-stage alteration and tin-tungsten
563 mineralization in the Khuntan Batholith, northern Thailand. *Journal of Asian Earth Sciences*, 21: 999-
564 1018

565 Yuan SD, Liu XF, Wang XD, Wu SH, Yuan YB, Li XK, Wang TZ (2012a) Geological characteristics and
566 ^{40}Ar - ^{39}Ar geochronology of the Hongqiling tin deposit in southern Hunan Province. *Acta Petrologica*
567 *Sinica* 28:3787-3797 (in Chinese with English abstract)

568 Yuan SD, Mao JM, Cook NJ, Wang XD, Liu XF, Yuan YB (2015) A Late Cretaceous tin metallogenic event
569 in Nanling W-Sn metallogenic province: Constraints from U-Pb, Ar-Ar geochronology at the Jiepailing
570 Sn-Be-F deposit, Hunan, China. *Ore Geology Reviews* 65:283-293.

571 Yuan SD, Peng JT, Hao S, Li HM, Geng JZ, Zhang DL (2011) In situ LA-MC-ICP-MS and ID-TIMS U-Pb
572 geochronology of cassiterite in the giant Furong tin deposit, Hunan Province, South China: New

573 constraints on the timing of tin-polymetallic mineralization. *Ore Geology Reviews* 43: 235-242

574 Yuan SD, Peng JT, Hu RZ, Li HM, Shen NP, Zhang DL (2008a) A precise U-Pb age on cassiterite from the

575 Xianghualing tin-polymetallic deposit (Hunan, South China). *Mineralium Deposita* 43:375-382

576 Yuan SD, Peng JT, Hu RZ, Bi XW, Qi L, Li ZL, Li XM, Shuang Y (2008b) Characteristics of rare-earth

577 elements (REE), strontium and neodymium isotopes in hydrothermal fluorites from the Bailashui tin

578 deposit in the Furong ore field, southern Hunan Province, China. *Chinese Journal of Geochemistry*, 27:

579 342-350

580 Yuan SD, Peng JT, Shen NP, Hu RZ, Dai TM (2007) ^{40}Ar - ^{39}Ar isotopic dating of the Xianghualing Sn-

581 polymetallic orefield in southern Hunan, China and its geological implications. *Acta Geologica Sinica*

582 (English Edition) 81:278-286

583 Yuan SD, Zhang DL, Shuang Y, Du AD, Qu WJ (2012b) Re-Os dating of molybdenite from the Xintianling

584 giant tungsten-molybdenum deposit in southern Hunan Province, China and its geological implications.

585 *Acta Petrologica Sinica* 28: 27-38 (in Chinese with English abstract)

586 Yuan YB, Yuan SD, Chen CJ, Huo R (2014) Zircon U-Pb ages and Hf isotopes of the granitoids in the

587 Huangshaping mining area and their geological significance. *Acta Petrologica Sinica* 30:64-78 (in

588 Chinese with English Abstract)

589 Yuan YB, Yuan SD, Liu XF, Mi JR, Xuan YS, Zhao PL (2014) Sulfur isotopic characteristics of

590 the Huangshaping granite and their geological significance in southern Hunan Province. *Acta Geologica*

591 *Sinica* 88: 2437-2442 (in Chinese with English Abstract)

592 Yuan YB, Yuan SD, Mao JW, Zhao PL, Yan C, Zhao HJ, Zhang DL, Shuang Y, Peng JT (2018) Recognition

593 of Late Jurassic W-Sn mineralization and its exploration potential on the western margin of the

594 Caledonian Guidong granite batholith, Nanling Range, South China: Geochronological evidence from

595 the Liuyuan Sn and Zhuyuanli W deposit. *Ore Geology Reviews*, 93: 200-210

596 Zhang D, Zhang WL, Wang RC, Chu ZY, Gong MW, Jiang GX (2015) Quartz-vein type tungsten
597 mineralization associated with the Indosinian (Triassic) Gaoling granite, Miaoshe area, northern
598 Guangxi. *Geological Review* 61:817-834 (in Chinese with English Abstract)

599 Zhang WL, Che XD, Wang RC, Zhang RQ, Yang Z (2014) Geochronological framework of the
600 Penggongmiao granite batholith. *Acta Geologica Sinica (English Edition)* 88:1041-1042

601 Zhang WL, Wang RC, Lei ZH, Hua RM, Zhu JC, Lu JJ, Xie L, Che XD, Zhang RQ, Yao Y, Chen J (2011)
602 Zircon U-Pb dating confirms existence of a Caledonian scheelite-bearing aplitic vein in the
603 Penggongmiao granite batholith, South Hunan. *Chinese Science Bulletin* 19:2031-2036

604 Zhang Y (2013) Geochronology and geochemistry of the igneous complex in the Gejiu, Yunnan Province.
605 (D) Beijing: The University of Chinese Academy of Sciences (in Chinese with English abstract)

606 Zhao JH, Zhou MF, Yan DP, Zheng JP, Li JW (2011) Reappraisal of the ages of Neoproterozoic strata in
607 South China: No connection with the Grenvillian orogeny. *Geology* 39: 299-302

608 Zhao KD, Jiang SY, Yang SY, Dai BZ, Lu JJ (2012) Mineral chemistry, trace elements and Sr-Nd-Hf isotope
609 geochemistry and petrogenesis of Cailing and Furong granites and mafic enclaves from the Qitianling
610 batholith in the Shi-Hang zone, South China. *Gondwana Research* 22: 310-324

611 Zhao PL, Yuan SD, Yuan YB (2016) Zircon LA-MC-ICP-MS U-Pb dating of the Xianglinpu granites from
612 the Weijia tungsten deposit in southern Hunan Province and its implications for the Late Jurassic
613 tungsten metallogenesis in the westernmost Nanling W-Sn metallogenic belt. *Geol. China* 43:120-131(in
614 Chinese with English Abstract)

615 Zhao PL, Yuan SD, Mao JW, Santosh M, Li C, Hou KJ (2016) Geochronological and petrogeochemical
616 constraints on the skarn deposits in Tongshanling ore district, southern Hunan Province: Implications

617 for Jurassic Cu and W Metallogenic events in South China. *Ore Geology Reviews* 78:120-137

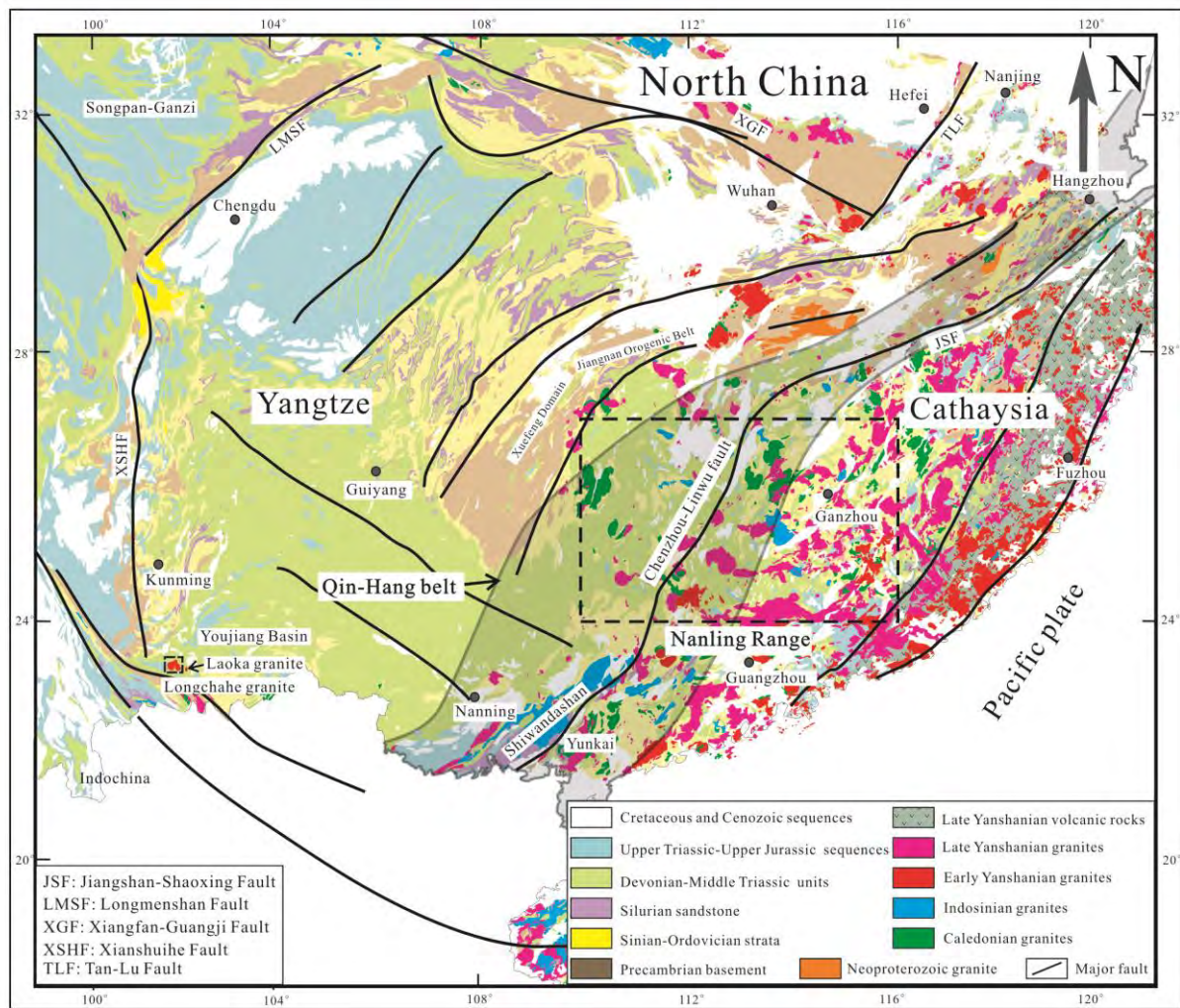
618 Zhou Y, Liang XQ, Wu SC, Cai YF, Liang XR, Shao TB, Wang C, Fu JG, Jiang Y (2015) Isotopic
619 geochemistry, zircon U-Pb ages and Hf isotopes of A-type granites from the Xitian W-Sn deposit, SE
620 China: Constraints on petrogenesis and tectonic significance. *J. Asian Earth Sci* 105:122-139

621 Zhu JC, Wang RC, Lu JJ, Zhang H, Zhang WL, Xie L, Zhang RQ (2011) Fractionation, evolution,
622 petrogenesis and mineralization of Laiziling granite pluton, Southern Hunan Province. *Geological*
623 *Journal of China Universities* 17:381 -392 (in Chinese with English abstract)

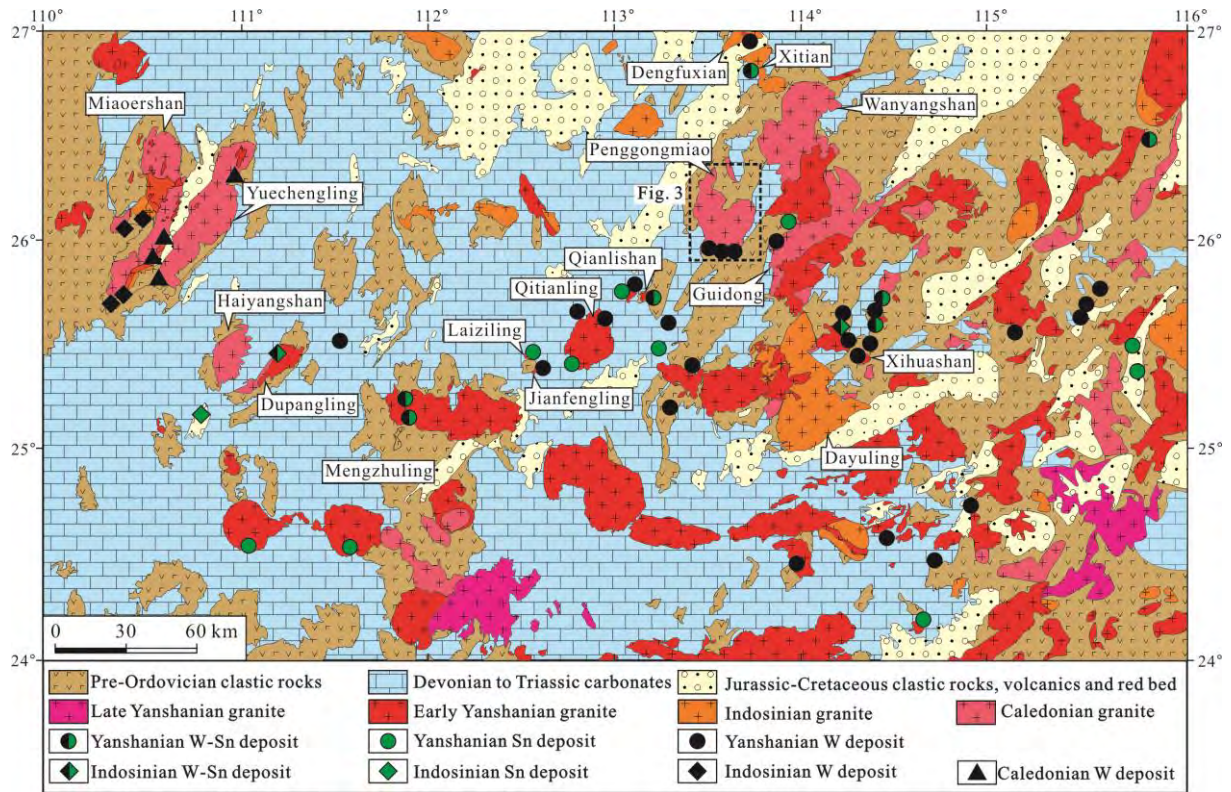
624 Zou XW, Cui S, Qu WJ, Bai YS, Chen XQ (2009) Re-Os isotope dating of the Ligufu tungsten-tin
625 polymetallic deposit in Dupangling area, Guangxi. *Geol. China* 36:837-844 (in Chinese with English
626 Abstract)

627

628 **Captions for Figures and Tables**



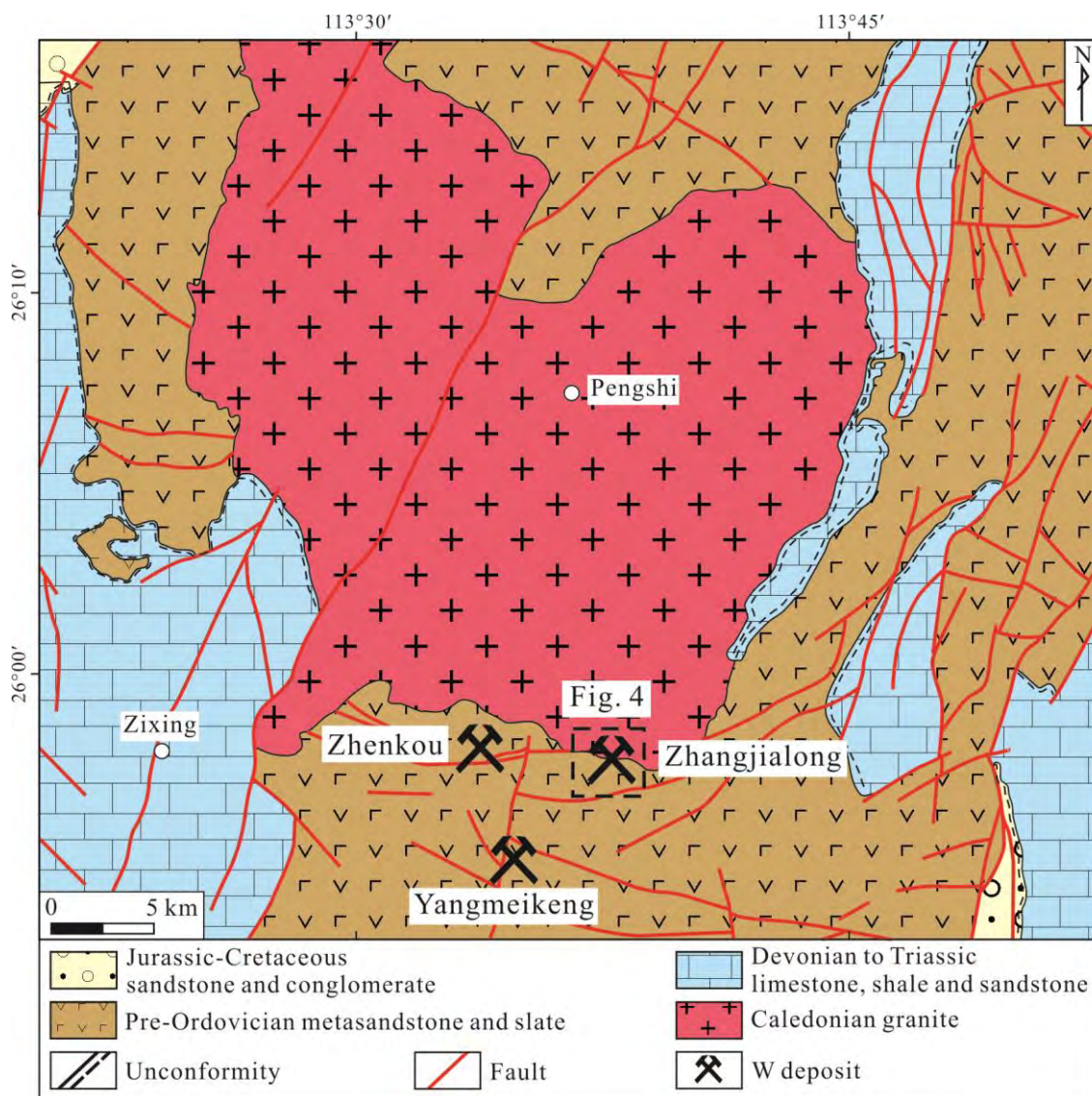
630 Fig. 1 Geological map of the South China Block (modified after Wang et al., 2013 and Zhou et al., 2006)



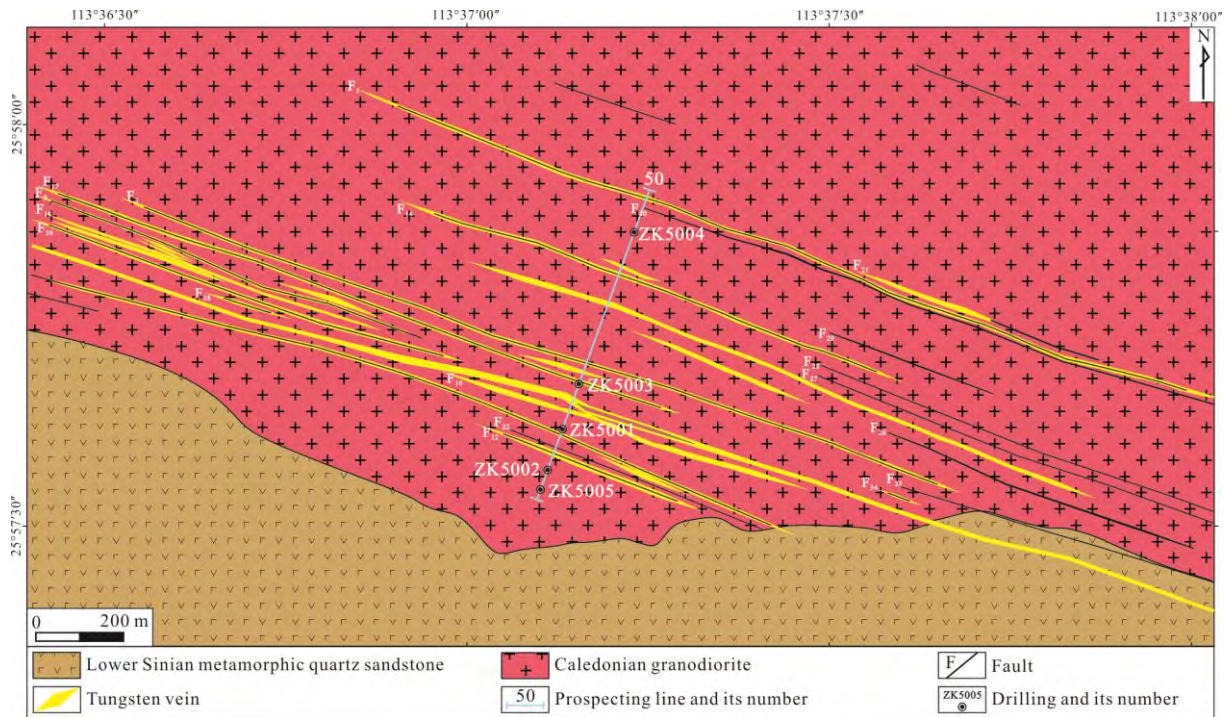
631

632 Fig. 2 Geological map of the Nanling Range showing the distribution of granites and associated tungsten/tin

633 deposits (modified after Mao et al., 2007).

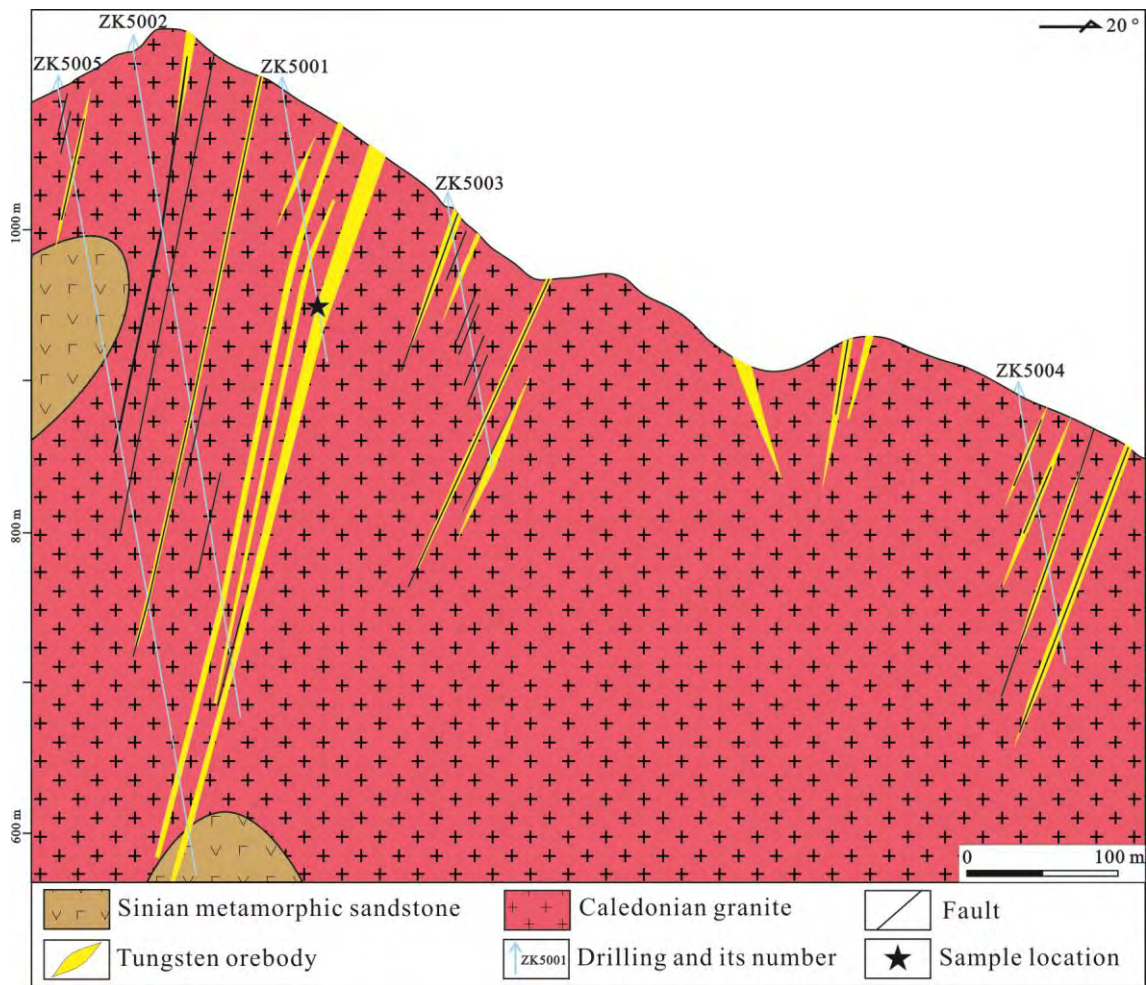


634
 635 Fig. 3 Geological sketch map of the Penggongmiao area, showing the distribution of tungsten deposits
 636 (modified after Li et al., 2013).



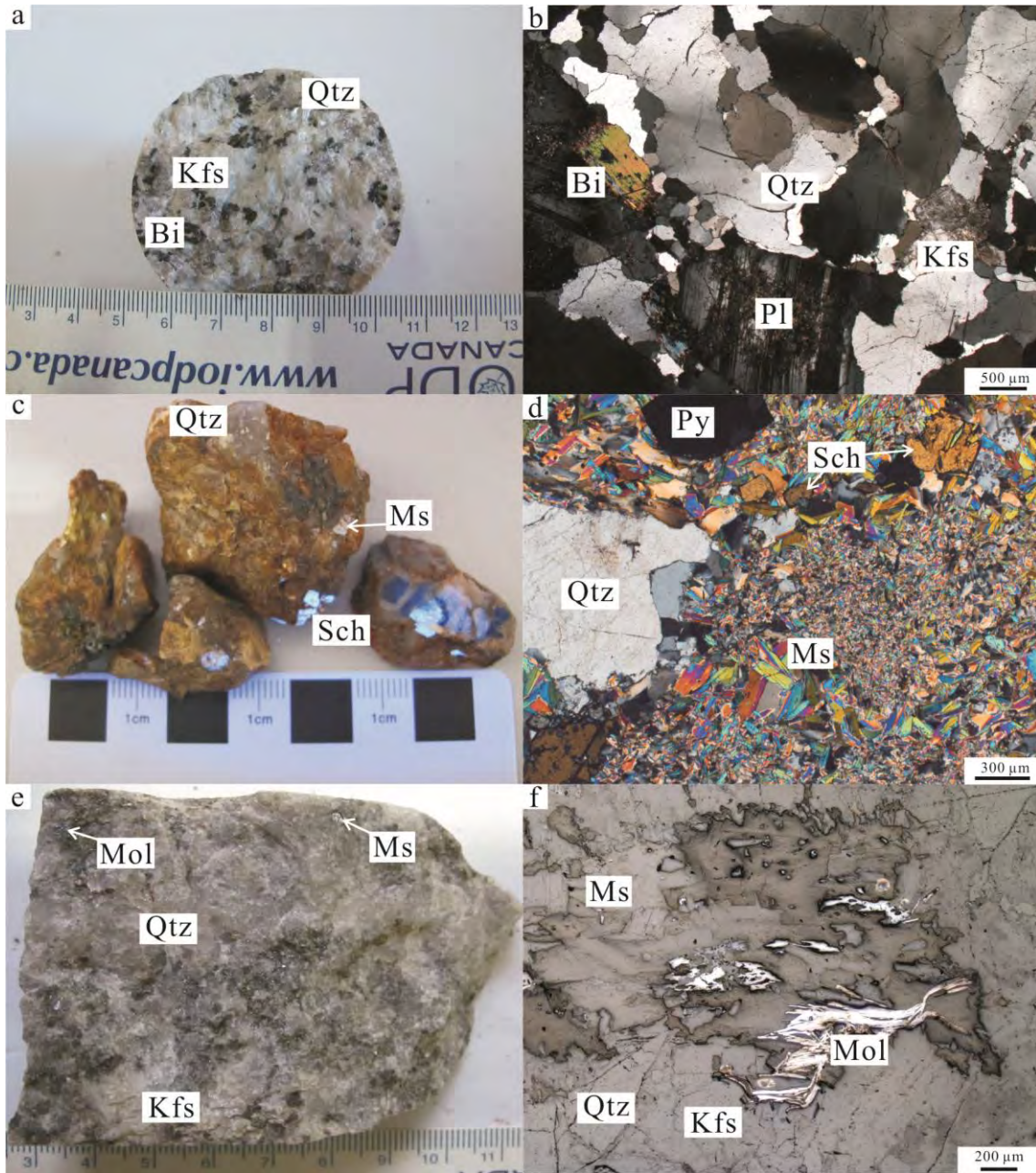
637

638 Figure 4 Geological sketch map of the Zhangjialong tungsten deposit (modified after Li et al., 2013)

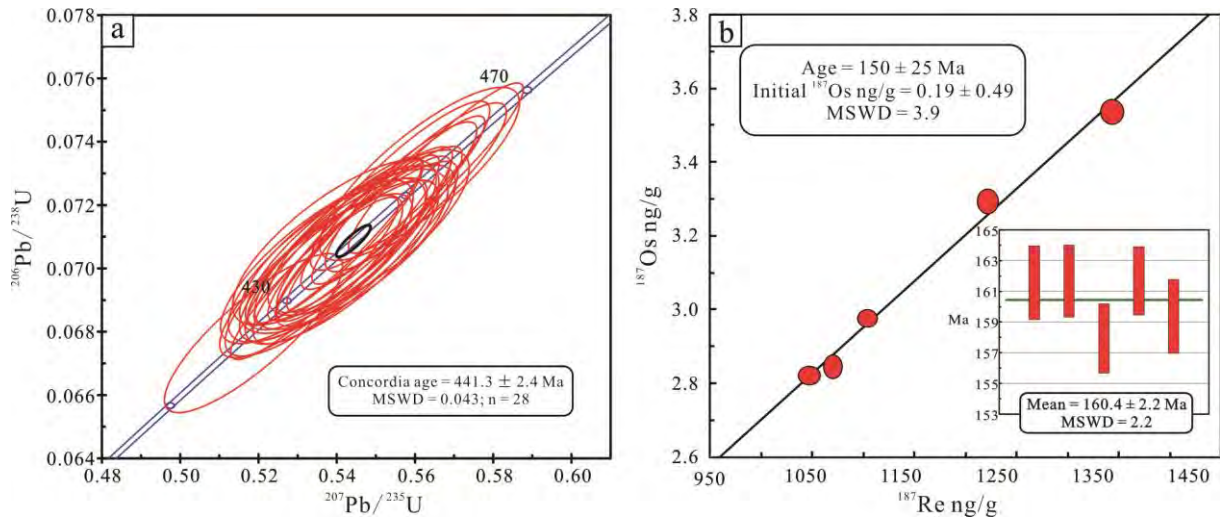


639

640 Fig. 5 Geological cross-section of No. 50 exploration line from the Zhangjialong tungsten deposit



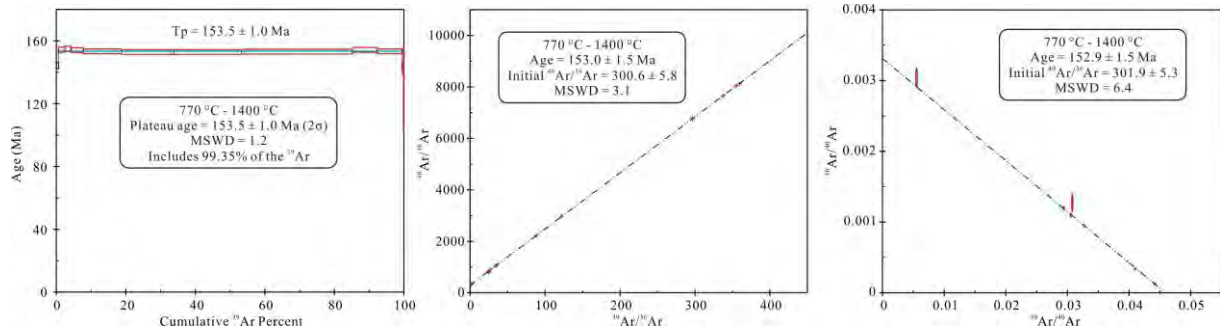
641
 642 Fig. 6 Photographs of hand specimens and micrographs of ore-hosted granite and molybdenite-bearing ores
 643 collected from the Zhangjialong W deposit. (a) and (b) medium coarse-grained biotite monzonite granite; (c)
 644 and (d) Greisen-type tungsten ore; (e) and (f) Molybdenite-bearing greisen-type tungsten ore.
 645 Ccp=chalcopyrite; Kfs= K-feldspar; Ms=moscovite; Pl=plagioclase; Py=pyrite; Qtz=quartz; Sch=scheelite.



646

647 Fig. 7 SIMS zircon U-Pb Concordia diagram (a) for the medium coarse-grained biotite monzonite granite

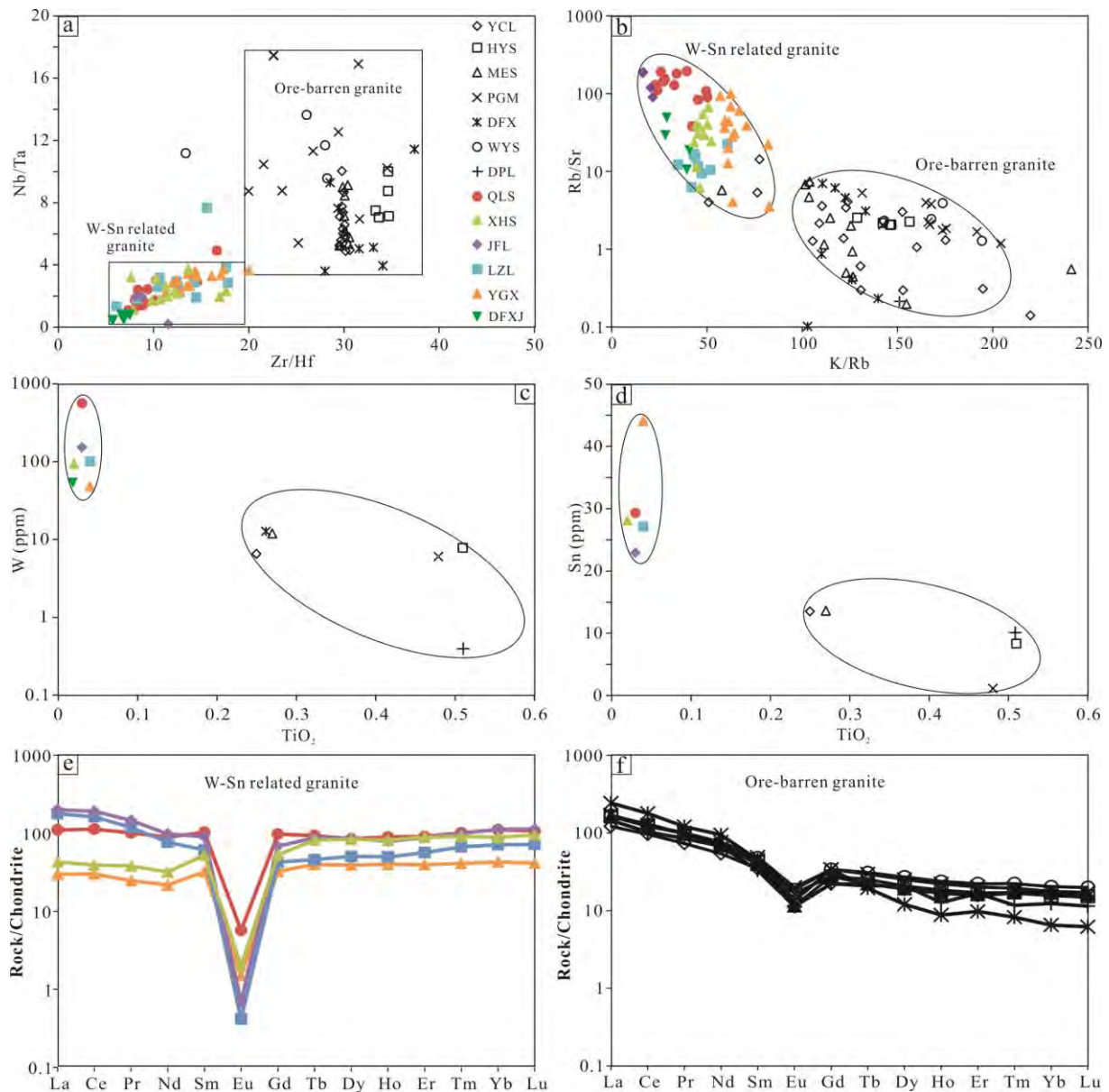
648 and Re-Os age (b) for molybdenite from the Zhangjialong W deposit.



649

650 Fig. 8 Plateau, isochron and inverse isochron ^{40}Ar - ^{39}Ar ages of muscovite from the greisen-type W ore in the

651 Zhangjialong W deposit.



652
 653 Fig. 9 Plot of (a) Nb/Ta versus Zr/Hf, (b) Rb/Sr versus K/Rb, (c)W versus TiO₂, (d) Sn versus TiO₂, (e) and
 654 (f) Chondrite-normalized REE patterns for W-Sn related granite and ore-barren granite for differentiating the
 655 barren granite batholiths and ore-bearing granitic stocks in the Nanling Range region (Data are from the
 656 references of Supplementary Table 4).

657



658

659 Supplementary Figure 1 Cathodoluminescence (CL) images of representative zircons separated from medium
 660 coarse-grained biotite monzonite granite of the Penggongmiao granite batholith. Also shown is the SIMS
 661 spot for U-Pb dating. The white bars are 100 μm in length for scale.

662

663 Supplementary Table 1 SIMS zircon U-Pb data of the biotite granite sample ZJL-2 in the Zhangjialong W
 664 deposit, Nanling Range.

665

666 Supplementary Table 2 ⁴⁰Ar-³⁹Ar data for muscovite from sample ZJL-2 of the Zhangjialong W deposit,

667 Nanling Range.

668

669 Supplementary Table 3 Re-Os isotopic data for molybdenites from the Zhangjialong W deposit, Nanling

670 Range.

671

672 Supplementary Table 4 Summary of the features of representative ore-barren batholiths and ore-bearing

673 stocks in the Nanling Range and surrounding area.

674